FOREX Publication
Open Access | Rapid and quality publishing

International Journal of
Electrical and Electronics Research (IJEER)
Research Article | Volume 11, Issue 2 | Pages 465-472 | e-ISSN: 2347-470X

Design and Control of a Tricycle with a Hybrid Electric Motor Cooling System Powered By Solar Photovoltaics

Jarapala Ramesh Babu[1*], Manas Ranjan Nayak[2] and B.Mangu[3]

[1,2]Department of Electrical Engineering, Biju Patnaik University of Technology Rourkela, Odisha, 769015, India, babu.ramesh444@gmail.com[1], manasnk72@gmail.com[2]

[3]Department of Electrical Engineering, University college of Engineering, Osmania University, Hyderabad, 500007, India, bmanguou@gmail.com[3]

***Correspondence:** Jarapala Ramesh Babu, Email: babu.ramesh444@gmail.com.

ABSTRACT- The power for a standard electric tricycle used for transportation comes from a battery, which can lose power after a certain amount of time. In this regard, the standard tricycle in the proposed concept will have a battery that will be charged by solar panels mounted on a stand on the rear of the tricycle. A solar-based renewable energy source is also used along with the traditional charging mechanism to make a hybrid system. The proposed tricycle is more stable in braking turns because it has a lower center of gravity compared to a bicycle. The proposed tricycle has movement in both directions, i.e., forward and reverse, for disabled persons. The proposed model was validated using the finite element analysis approach in solid work for different points of the frame and different types of loads. Also Electric motors have a great efficiency of operation, but they create a lot of heat depending on the torque and speed they need to run. As a result, an effective motor cooling system is required to keep the temperature within restrictions. Although the coolant pump and radiator fan in a conventional motor liquid cooling system do an efficient job, they are also energy hogs. The FEA approach was used to identify the maximum stress, displacement, and safety factors.

Keywords: Solar Power, Battery, Finite element analysis, solid work, tricycle, BLDC motor.

ARTICLE INFORMATION

Author(s): Jarapala Ramesh Babu, Manas Ranjan Nayak and B.Mangu;

Received: 06/09/2022; **Accepted**: 21/01/2023; **Published**: 30/06/2023;
E- ISSN: 2347-470X;
Paper Id: IJEER220611;
Citation: 10.37391/IJEER.110229
Webpage-link:
https://ijeer.forexjournal.co.in/archive/volume-11/ijeer-110229.html

Publisher's Note: FOREX Publication stays neutral with regard to jurisdictional claims in Published maps and institutional affiliations.

1. INTRODUCTION

Automobiles, buses, trains, and motorcycles are all modes of transportation that have a number of negative consequences for their users and the environment. The expense, air pollution, and health hazards associated with these difficulties might all be different[1] [2]. According to the Washington Post, 13 billion people do not have access to electricity around the world. This is due to the high cost of electrical sources, which many countries are unable to afford to offer their citizens. Furthermore, car exhaust contributes to air pollution, which is harmful to the environment. Furthermore, long-term use of automobiles, motorcycles, and various forms of public transit will result in obesity due to the lack of activity that these modes of transportation provide. In fact, the World Health Organization estimates that about 650 million individuals are obese. Bicyclists utilise their tricycles to get from one point to another all over the world, and many of them use tricycles to travel. As a result, it's critical to devise a method for these bikers to relax during their long-distance journeys. As a result, developing a new clean, renewable, and healthier mode of transportation is one of the most pressing issues facing engineers today. As engineering students, we think that using solar energy and a dynamo to power a hybrid (electric and manual) tricycle can be a cheap and easy way for people to get around on a daily basis[3].

The Central Mechanical Engineering Research Institute in Kolkata designed it as an alternative to auto rickshaws powered by IC engines. A solar-powered charging system was also incorporated into the prototype[4]. One shock absorber and a flashlight were included in the suspension system to make night time riding more comfortable. This could also be beneficial in a foggy or rainy environment to improve visibility. Additionally, the back wheels could be driven manually or by a motor. The vehicle had a maximum weight capacity of 200 kg and a maximum speed of 15 km/h[5].

The major drawback of conventional wheelchairs is their characteristic feature of the necessity of manual operation with a handheld rotary pedal [6] [7]. Hence, the electric wheelchair was introduced to overcome the necessity of manual operation with a handheld rotary pedal. However, an electric wheelchair requires rechargeable batteries to be operated, and his major drawback of an electric wheelchair vehicle is its incapability to travel longer distances due to inadequate battery life. In addition, disabled people operating the electric wheelchair vehicle may not be able to plug in the charger to recharge the batteries. Hence, in this paper, a three-wheeler hybrid electric vehicle based on solar energy is proposed.

These approaches include air cooling, liquid cooling, heat pipes, and hybrid cooling are some examples of these methods. Air

FOREX Publication
Open Access | Rapid and quality publishing
International Journal of Electrical and Electronics Research (IJEER)
Research Article | Volume 11, Issue 2 | Pages 465-472 | e-ISSN: 2347-470X

conditioning is simple to build and set up, but it may not provide enough cooling. An additional drawback is the inefficiency and impossibility of direct control of a cooling fan that is often attached to the motor shaft [8],[9]. The liquid cooling system's coolant pump and radiator fan use a lot of energy, despite the system's efficiency. However, the addition of liquid cooling lines increases both the system's size and complexity. The amount of heat that can be carried by a heat pipe is limited by parameters like the capillary limit, fluid characteristics, operating temperatures, and so on, even if heat pipes may function passively in the presence of a temperature gradient.

In this proposed tricycle, a power converter and microcontroller are used for energy management between solar PV, battery, and load. Where the bicycle is operated manually. For disabled people, the proposed tricycle allows vehicle movement in both directions, i.e. forward and reverse. The bicycle, on the other hand, can only move forward. Further, a solar-based renewable energy source is used along with the conventional charging mechanism, which forms a hybrid energy system. In contrast, an energy source is used in bicycle batteries. In comparison to a bicycle, the proposed tricycle is more stable in braking turns by reducing the Centre of gravity. It is built to provide safety, shelter, and comfort to the rider, but bicycle safety is lacking. A BLDC hub motor mounted in the front wheel housing powers the solar-assisted tricycle, whereas a PMDC motor mounted separately on the rear wheel powers the bicycle.

The key contributions to the work are as follows:

1. In the present invention, a conventional electric mobility locomotive for disabled people (partially or completely) is redesigned as a hybrid electrical tricycle in order to provide an uninterrupted travelling experience to the user, which fulfils the need of the hour in society.
2. Further, a solar-based renewable energy source is used along with the conventional charging mechanism to form a hybrid system, which is disclosed.
3. Create a battery-operated, electric-motor tricycle capable of 25 kilometres per hour in speed.
4. The goal of this redesign was to create a tricycle with a lower centre of gravity, making it much more stable during braking bends.
5. Also, solar power generates almost 108 units annually, which results in a reduction of 58.104 kg of coal and 116.177 kg of CO_2 emissions.
6. Prior to production, a finite element analysis evaluation of the frame's structural integrity is performed. Safety, ergonomics, weight reduction, and chassis production cost were all factors that were taken into account.
7. To make the production vehicle wheelchair-free for people with disabilities who have problems with their legs.

2. PROPOSED DESIGN AND IMPLEMENTATION

In an embodiment of the present disclosure, a hybrid electrical tricycle is disclosed. The A hybrid electrical tricycle predominantly comprises of a solar panel, two 12V, 14Ah batteries, one 12V, 12Ah battery, a 250W hub motor positioned at the front wheel, a right-side rear wheel positioned at the right side with a crank gear using a drive chain, a left rear wheel, left throttle, right throttle, motor controller, and an LED light with a key lock battery indicator.

Figure 1 portrays the hybrid electrical tricycle unit devised as per the embodiment of the present disclosure and the controller architecture for a hybrid motor cooling system. In the present disclosure, an electric tricycle unit comprises mechanical and electrically powered elements. Whenever the user tries to move the electric tricycle without unlocking the key, an anti-theft alarm is activated through the buzzer. Further, when the electric tricycle is unlocked using a mechanical key, the motor controller gets ready to drive the hub motor. Subsequently, the right throttle needs to be operated at the desired speed levels using a speed level switch. Further, a sound horn is provided for alerting others while driving the electric tricycle. Significantly, the electric tricycle made it more reliable to operate manually using the pedal connected to the crank gear through the crankshaft and drive chain. Moreover, three metal bolts are used to fix the seat of the electrical tricycle unit.

(a)

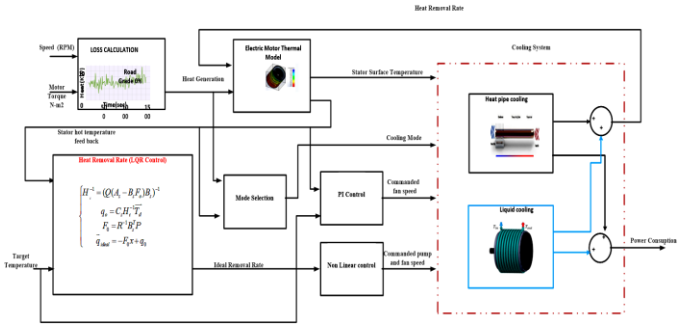

(b)

Figure 1: Tricycle chassis as a tool for (a) design exploration (b) Controller architecture for a hybrid motor cooling system

2.1 Mathematical Models

Mathematical models of the electric motor, heat pipes, and air and liquid cooling subsystems have been created to describe the heat transfer and removal processes of the proposed electric motor hybrid cooling system. Developing the models required some educated guesswork.

A1: We disregard the resistance of thermal contacts.

A2: The insulation around the motor is second to none.

A3: The effect of the fin cover on convective heat transmission is disregarded.

A. Thermodynamic Model of a Reduced-Order Electric Motor

Figure 1(b) depicts the components of a typical electric motor, including the stator through windings, the rotor through

FOREX Publication
Open Access | Rapid and quality publishing
International Journal of Electrical and Electronics Research (IJEER)
Research Article | Volume 11, Issue 2 | Pages 465-472 | e-ISSN: 2347-470X

permanent magnets, and the casing. The motor's internal temperatures at various phases of operation should be predictable using the thermal model. Zhou et al. designed a thermal model of a lower order for use in electric motor drive powertrains. Wang et al. developed a more precise thermal model by accounting for air-gap heat convection inside the motor. The internal temperature field of a 40-state stator and 20-state rotor UQM Power Phase 145 electric motor was investigated. Initial state space matrices were constructed using finite element analysis (FEA).

As can the stator windings often reach the motor's greatest temperature owing to the strong current flow there. In order for convective heat transfer to occur, an air gap must be present between the rotor and stator. The internal passion transfer of an electric motor may be represented by the following expression:

$$d\left(\frac{dT}{dt}\right) - k\nabla^2 T = q \quad (1)$$

Where T represents the temperature and d, k, and k, respectively, represent the specific heat and thermal conductivity of the material. The heat flow, denoted by q, is the input variable into the system.

By using finite element analysis methods, we may further discretize *equation (1)* into an ordinary differential equation, as follows:

$$D \underset{T}{\rightarrow} + K \underset{T}{\rightarrow} = \underset{q}{\rightarrow} \quad (2)$$

In the finite element mesh, the matrices D, K represent the precise heat and thermal conductivity, while the scalar matrix T represents the nodal temperature. Factors such as the conductor, the core, friction, the permanent magnet, windage losses, and convective heat transfer at the machine's edges all have an impact on the excitation vector q of an electric motor. The motor stator (t_s) and rotor (t_r) vectors may be used to rewrite *eq. (2)* in state space with a different basis and lower model order.

$$\dot{\underset{x_s}{\rightarrow}} = A_s \underset{x_s}{\rightarrow} + B_s \underset{q_s}{\rightarrow}$$
$$\underset{x_s}{\rightarrow} = C_s \underset{x_s}{\rightarrow} + D_s \underset{q_s}{\rightarrow} \quad (3)$$

$$\dot{\underset{x_r}{\rightarrow}} = A_r \underset{x_r}{\rightarrow} + B_r \underset{q_r}{\rightarrow}$$
$$\underset{x_r}{\rightarrow} = C_r \underset{x_r}{\rightarrow} + D_r \underset{q_r}{\rightarrow} \quad (4)$$

Where x_s, A_s, B_s, C_s, and D_s are the standard vectors and matrices of a state space.

The rotational speed and torque of the motor inform the heat flow vectors, q_s and q_r, which are used as inputs to the model. The temperature distribution of an electric motor may be calculated in terms of q_s and q_r using FEA. The problem of varying temperatures throughout a grid may be addressed.

B. A Thermal Model of a Heat Pipe

The thermal cradle has heat pipes arranged in a circle to dissipate the heat produced by the electric motor. In order to derive a model with a single set of parameters, one must first determine the thermal resistance, R_{cra}, expressed as

$$R_{cra} = \frac{t_{cra}}{A_{cra}K_{cra}} \quad (5)$$

This formula includes the cradle thermal conductivity K_{cra}, the average radial interaction area A_{cra}, and the cradle thickness t_{cra}. It is necessary to represent both the v_{apour} movement and heat transmission in a heat pipe. The compressible version of the Navier-Stokes equation describes the motion of v_{apour}. However, the heat transfer mechanism is of primary relevance, hence the fluid dynamics will not be described. A thermal cradle is used to hold the heat pipe evaporators. The thermal resistance of the cradle and the E-motor thermal model may be used to determine the temperature of the cradle.

A simplified expression for the heat transmission between the heat pipe shell, the wick structure, the interior v_{apour}, and the connected fins is

$$\rho C_p \nabla T + \nabla_q = Q,$$
$$q = -k\nabla T \quad (6)$$

The density, C_p, fluid (heat pipe Vapour) velocity, thermal conductivity, and heat source are all represented here by p, u, k, and Q, respectively.

The sintered copper powder and water in the heat pipe wick construction create a porous substance. By introducing the idea of an effective thermal conductivity, or K_{eff}, we might be able to simplify how heat moves through a wick, which would lead.

$$k_{eff} = k_s\left(\frac{2+k^*-2\emptyset(1-k^*)}{2+k^*+\emptyset(1-k^*)}\right) \quad (7)$$

The thermal conductivity of copper is denoted by k_s and that of water by kl; the ratio of the two is denoted by k. The symbol denotes the wick's porosity. Because they use phase change and latent heat, heat pipes are classified as superheat transfer devices. Infrared heating wick, the proposed location of the phase change is at the point of contact with the vapor. Latent heat may be calculated using the mass flow rate of evaporating and condensing water.

With the help of the connected fins, heat may be dissipated by convection. For this reason, the heat flux output may be written as

$$q_{out} = h_{air}(T - T_{amb}) \quad (8)$$

Where T_{amb} is the ambient air temperature and T is the heat exchanger temperature (the fins and heat pipe condenser shell). The Nusselt number and heat exchanger shape are two examples of how the convective heat transfer coefficient, or "Hair," changes.

$$h_{air} = \frac{N_u k_{air}}{S} \quad (9)$$

The distance between two neighbouring fins, denoted by S, and the thermal conductivity of air, denoted by K_{air}, are other important characteristics. The N_{ussel}t number, in the case of natural convection, may be written as

$$N_{u_n} = \frac{1}{24}R_a\left(\frac{S}{L}\right)\left(1 - e^{\frac{35}{R_a\left(\frac{S}{L}\right)}}\right)^{0.75} \quad (10)$$

FOREX Publication
Open Access | Rapid and quality publishing
International Journal of Electrical and Electronics Research (IJEER)
Research Article | Volume 11, Issue 2 | Pages 465-472 | e-ISSN: 2347-470X

Ra is the Rayleigh number, and L is the length of the fin in the direction of gravity. The nusselt number for forced convection is given by [22]

$$N_{u_n} = \left(\frac{1}{(0.5+RePr)} + \frac{1}{(0.664\sqrt{Re}Pr^{0.33}\sqrt{1+3.65/\sqrt{Re}})^3} \right)^{-0.33} \quad (11)$$

The Reynolds number, which is represented by the symbol Re, depends on how fast the air is moving (Va), how far apart the fins are (b), and how sticky the air is (V).

It is possible to represent a single heat pipe with fins by making use of symmetry. Conditions such as air velocity, evaporator temperature, and room temperature are sent into the system. By integrating the heat output flux from *eq. (8)* over the entire fin surface area surrounding the heat pipe, it is possible to determine the amount of heat the system extracted. Q_{hp} is the total amount of heat rejected by all of the heat pipes in a system, and it may be calculated by multiplying n, the number of heat pipes.

$$Q_{hp} = n \int q_{out} \partial A_{fm} \quad (12)$$

The amount of heat extracted is calculated using a 3D lookup table that takes input from the system.

C. The Model of Liquid Cooling

The electromechanical actuators in the liquid cooling subsystem are the water pump, which may be adjusted in speed, and the radiator fan. Since the four motors are all operating at the same speed, torque, and temperature, the coolant flow may be considered to be distributed equally among them. Therefore, this research focuses on only one kind of motor.

Cradle liquid is cooled by a spiral coolant jacket on the outside of the support structure. Because of this, T_{cra}, the average surface temperature of the cradle's exterior, rises.

$$T_{cra} = T_{so} - Q_{hp} R_{cra} \quad (13)$$

Where Tso is the stator surface temperature and Q_{hp} is the heat pipe efficiency in *equation (12)*.

T_{in} and T_{out} are still taken into account even if the coolant temperature within the motor casing varies. One possible method of calculating the heat transfer from the electric motor to the coolant is as follows: Q_{mc}.

$$Q_{mc} = min\{h_{lip}(T_{cra} - T_{in}),\ C_{pv}\dot{m_{mot}}(T_{cra} - T_{in})\} \quad (14)$$

Where the heat transfer coefficient of the coolant (h_{liq}) and C_{pw} is the coolant's heat capacitance. The symbol m_{mot} stands for the mass flow rate of cooling fluid for one motor.

As a way to express the predicted increase in coolant temperature, we may use the formula

$$\frac{dT_{out}}{dt} = \frac{Q_{mc}}{M_{wm}C_{pw}} - \frac{\dot{m_{mot}}}{M_{wm}}(T_{out} - T_{in}) \quad (15)$$

Where the mass of the jacket's coolant (M_{wm}). The quantity of coolant in the outerwear Together, the four motor streams exit and enter the radiator.

Q_{liq}, the heat transfer rate for liquid cooling, may be determined using the following formula:

$$Q_{lip} = h_{lip} \Delta T_m A_{cra} \quad (16)$$

Where T_c is the coolant temperature and Tm is the average logarithmic temperature difference between the thermal cradle and the coolant,

$$\Delta T_m = \frac{T_{in} - T_{out}}{In[(T_{in} - T_{out})/(T_{cra} - T_{in})]} \quad (17)$$

Since Q_{rem} is cooling system removes all of the heat it generates concluded heat pipes and perhaps coolant motion,

$$Q_{rem} = \begin{cases} Q_{hp} & , \dot{m_{pump}} = 0 \\ Q_{hp} + Q_{lip}, & \dot{m_{pump}} > 0 \end{cases} \quad (18)$$

Where m_{pump} is the fluid flow rate of the coolant pump, which is four times that of m_{mot}.

D. Estimating the Energy Use of a Cooling System

A knowledge of the cooling system's power consumption is necessary for any evaluation of its effectiveness. The cooling fans and pump use the most power. If you want to calculate how much energy that centrifugal fan consumes, you may do it as follows:

$$E_{fan} = C_{fan} \left(\frac{N_{fan}}{60} \right)^3 \quad (19)$$

And N_{fan} is the number of revolutions per minute of the fan. Shaft speeds may be used to describe the flow rates and power consumption of the coolant pump and the radiator fan.

$$\dot{m_{pump}} = \frac{N_p D_{is} \rho_w}{60},$$
$$E_{pump} = {D_{is}}^3 \rho_w \left(\frac{C_{p,rad}}{A_{flow}} + \rho_w C_{p,pipe} \right) \left(\frac{N_p}{60} \right)^3 \quad (20)$$

$$\dot{m_a} = \frac{{D_{rfan}}^3 C_{flow} N_{rfan} \rho_a}{60},$$
$$E_{rfan} = {D_{rfan}}^5 C_{flow} C_{pres} \rho_a \left(\frac{N_{rfan}}{60} \right)^3 \quad (21)$$

The values of A_{flow}, C_{flow}, C_{pres}, $C_{p,pipe}$, D_{is}, ρ_a, and $\rho_w$are considered constant.

2.2 Finite Element Analysis (FEA)

Solidworks is the software used to create the CAD model and run the simulation. SolidWorks allows you to create both 2D and 3D models. Part design is the first phase of component design, followed by assembly[10] [11]. Surfaces, edges, and faces can be used to create 3D geometries in SOLIDWORKS component models. The tricycle model made with 3D geometrical tools has beams, weldment joints, surfaces, edges, and other parts in it.

The tricycle's frame is comprised of hollow pipes joined together with welded connections. The front pipe, which will give interior space for the steering pipe, must bear a greater

FOREX Publication
Open Access | Rapid and quality publishing
International Journal of Electrical and Electronics Research (IJEER)
Research Article | Volume 11, Issue 2 | Pages 465-472 | e-ISSN: 2347-470X

weight than the other pipes, hence it is larger. The vertical pipes linked to the vehicle's rear side, which will carry the rider's load, are likewise made larger than the other pipes. Further analysis would show that all of the other pipes are smaller and that they are sufficiently strong. The frame's design is depicted in *figure 2*.

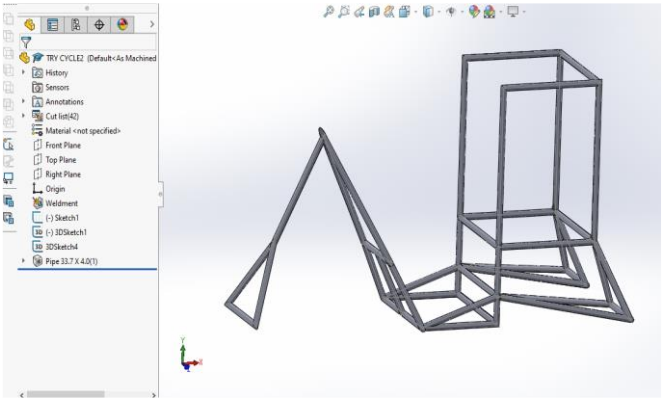

Figure 2: 3-D model of tri cycle body frame

2.3 Material for frame

For the frame's construction, aluminum alloy was used. The most commonly used metal for frame construction is aluminum alloy. Steel is another commonly used component material. In comparison to structural steel, however, aluminum alloy may be less expensive, lighter in weight, and more reliable in table 1. The frame must be able to handle loads such as bending, torsion, lateral loads while braking, and distant loads while steering [12] [13] [14].

Table 1. Properties of Aluminum Alloys

Properties	Value	Units
Elastic Modulus	70000	N/mm^2
Poisson's Ratio	0.33	N/A
Modulus of Shear	25900	N/mm^2
Density of Mass	2680	Kg/m^3
Tensile Strength	290	N/mm^2
Compressive Strength		N/mm^2
Yield Strength	255	N/mm^2
Thermal Expansion coefficient	2.38e^{-05}	/K
Thermal Conductivity	137	W/(m.k)
Specific heat	880	J/(kg.K)
Material Damping Ratio		N/A

2.3 Control Strategies

The controller maintains a safe stator temperature in the electric motor by adjusting the speeds of the pump and fan. This has the added benefit of lowering the systems overall power consumption. The electric motor state-space thermal model takes as inputs the stator and rotor heat fluxes, q_s and q_r, respectively. Since the internal rotor of the motor is not connected to the cooling system in any direct way, q_r cannot be regulated. The two heat exchangers in the cooling system need a mode switching plan[15],[16].

The heat pipes are cooled by a centrifugal fan, whose speed is modulated by a classical controller.

$$N_{fan} = K_p\left(T_{ref} - T_{sh}\right) + K_I \int \left(T_{ref} - T_{sh}\right)dt \quad (22)$$

Where T_{sh} represents the average of the stator hot temperature, which is the state vector elements numbered two through twelve. K_p and Ki are the controller gains. Since the voltage across the fan motor is related to the rotational speed of the fan, once the fan speed is known, the actual control input (such as the fan motor voltage, V), may be calculated.

A liquid cooling subsystem may be engaged to remove excess heat from the motor if the heat generation rate is too high for the heat pipes to manage. For the most part, the stator windings of an electric motor are where the heat is concentrated. The optimal heat removal rate may be determined while simultaneously decreasing the size of the temperature vector at the thermal model's output. The cost function, J, for which an optimum controller is developed is as follows:

$$J=\int_{t_0}^{t_f}\left(\left(\underset{x_s}{\rightarrow} - \underset{T_d}{\rightarrow}\right)^T Q \left(\underset{x_s}{\rightarrow} - \underset{T_d}{\rightarrow}\right) + q_s R \underset{q_s}{\rightarrow}\right) \quad (23)$$

Where T is a temperature vector used as a standard by electric motors. Positive diagonal weighting matrices, Q and R, are what we're talking about here.

$$Q_{ij} = \begin{cases} P_Q; i = j \cap 2 < i < 12 \\ 0; otherwise \end{cases}$$
$$R_{ij} = \begin{cases} P_R; i = j = 1,2,4,5 \\ 1; i = j = 3 \\ 0; otherwise \end{cases} \quad (24)$$

In which P_Q and P_R are positive quantities. As shown in this research, Q is meant to maintain a consistent temperature in the electric motor stator between the indices 2nd and 12th.
Similarly, the sole modifiable output is the third component of the input vector q s, which signifies the heat elimination flow by the cooling method.

The ideal architecture of a controller looks something like

$$\begin{cases} {H_c}^{-1} = (Q(A_s - B_s F_o)^{-1} \;\; ; F_o = R^{-1}{B_s}^T P \\ q_o = C_s {H_c}^{-1} \underset{T_d}{\rightarrow}; \underset{q_{ideal}}{\longrightarrow} = -F_o x + q_o \end{cases} \quad (25)$$

Where P is the answer to the Riccati calculation. The thermal removal rate (Q_{ideal}) of an ideal heat cooling system may be determined using the following formula:

$$Q_{ideal} = [0\ 0\ 1\ 0\ 0] \underset{q_{ideal}}{\longrightarrow} A_{cra} \quad (26)$$

Where Q_{ideal} is the theoretical maximum heat flow. Using eliq and a time derivative, we can calculate the tracking error for heat rejection during liquid cooling:

$$e_{lip} = Q_{ideal} - Q_{rem}, \frac{de_{lip}}{dt} = -k_e e_{lip} \quad (27)$$

In this case, Ke represents a positive control gain. The time-derivative of heat loss from liquid cooling, as calculated by

FOREX Publication
Open Access | Rapid and quality publishing
International Journal of Electrical and Electronics Research (IJEER)
Research Article | Volume 11, Issue 2 | Pages 465-472 | e-ISSN: 2347-470X

$$\frac{dQ_{lip}}{dt} = \frac{d(Q_{ideal} - Q_{hp})}{dt} + k_e e_{lip} \quad (28)$$

In *eq. (16)* and *(17)*, the derivative of the rate of heat loss due to liquid cooling is shown by the log mean temperature.

$$\frac{dQ_{lip}}{dt} = \frac{\partial h_{lip}}{\partial \dot{m}_{mot}} \frac{\partial \dot{m}_{mot}}{dt} A_{cra} \Delta T_m + h_{lip} A_{cra} \frac{d\Delta T_m}{dt} \quad (29)$$

Plugging these values into a control law for the coolant mass flow rate yields *eq. (29)* into *eq. (28)*, yielding. Since mass flow rates are proportional to pump and fan speeds, we may get them from *eq. (20)* and *eq. (21)*, respectively. Based on the proportional relationship, the actual control inputs (such as the voltages of the pump and fan motors, V_{pump} and V_{rfan}) may be calculated once the pump and fan speeds are known.

2.4 System Design Calculations

Diameter of the wheel is 600mm = 0.6m
Radius of the wheel r= 0.3m
Average speed of the tri-cycle=V=25km/hr

Force calculation

Force F=m*g in Newton
Where g=9.81 is the acceleration.

2.5 Analysis of Co2 Reduction through the Solar Array

One kilogram of coal emits 2.86 kg of CO_2, thereby increasing the carbon footprint which in turn contributes to global warming [17] [18] [19].CO_2 Emission by Three-wheel HEV is 116.177 kg .

3. RESULT AND DISCUSSION

The results of all the analyses performed with Finite Element Analysis methodology include mesh element results, bending case results, Torque case results, sum of Human weight and battery weight also with torque case results, sum of Human weight and battery weight also with torque case results, sum of Human weight and battery weight also with torque case results, and solar panel load case results. Furthermore, the frame FEA methodology yields maximum stress, maximum displacement, and a factor of safety.

Static Analysis

i. Model meshing
ii. Fixed boundary condition
iii. Boundary condition applied in the form of loads
iv. Results Study (a) stress Analysis (b) displacement analysis

3.1 Model of Mesh

Without meshing, a simulation cannot be run. Meshing is the first step in the simulation process, since it is what generates the finite elements that make up a finite element model for use in a FEA. Model meshing is the process of dividing up your geometry into smaller pieces, or finite elements. Now, let's establish some terms:
In contrast to limitless, finite refers to a specific amount.
Element: A simple, present shape component or block.
The model's essential components are the elements. Meshing breaks down a complex problem into a finite number of parts (finite) of a shape that can be easily calculated (elements).

In Solid Works Simulation, creating a mesh is simple. To begin, right-click on the mesh icon in the Simulation Tree and select Create Mesh from the menu that appears. You don't look at any alternatives or even numbers when doing a quick mesh. Only a slider for controlling the density or size of the elements is visible. In terms of element size, fine is to the right and coarse is to the left. A fine mesh will have smaller elements than a coarse mesh, which will have fewer or larger elements.

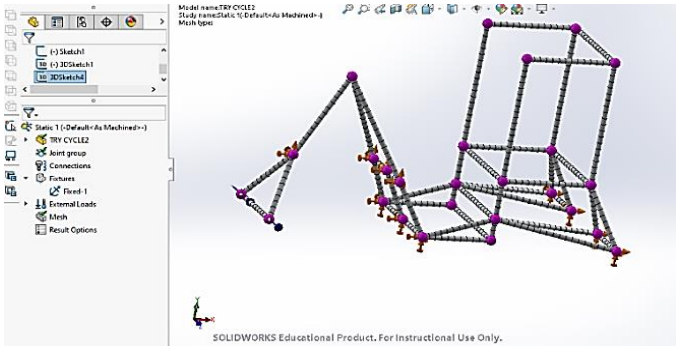

(a)

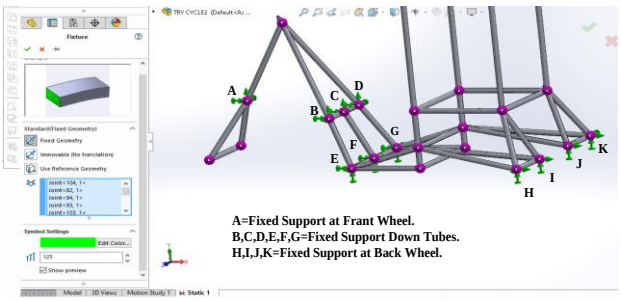

(b)

Figure 3: (a) Fixed Boundary Conditions (b) Fixed Boundary Conditions with Points

For FEA approach, boundary conditions of CAD model of attempt cycle Frame Solid Works are used to perform Finite Element Analysis on the frame of an electrical tricycle. Two studies are performed on the CAD model of the frame that is stored in SOLID WORKS. Stress, displacement with and without deformation cases (true and automated cases) are the names given to both analyses. Different analyses were carried out with various forces and fixtures shown in *figure 3(a)-(b)*. *Figure 4* depict the Vehicle speed, Motor Torque and Constant Motor Temperature using Hybrid cooling system at constant Temperature using hybrid cooling system.

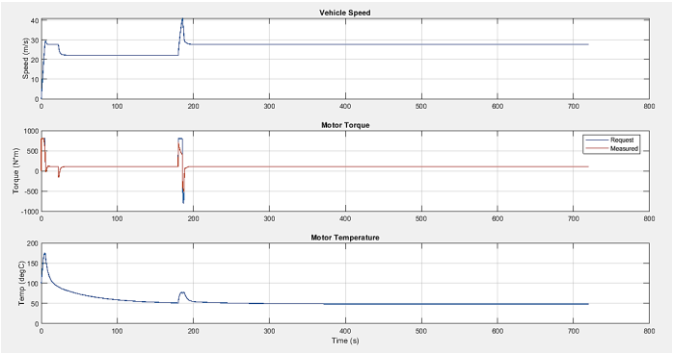

Figure 4: Vehicle speed, Motor Torque and Constant Motor Temperature

FOREX Publication
Open Access | Rapid and quality publishing
International Journal of Electrical and Electronics Research (IJEER)
Research Article | Volume 11, Issue 2 | Pages 465-472 | e-ISSN: 2347-470X

3.2 Sum of Solar panel, human, battery, and Motor Torque loads

Figure 5(a) - (e) depict the sum of the solar panel, human, battery, and motor torque loading modes of a tri-cycle frame. The boundary condition is the pre- and post-constraint degrees of freedom of the frame in the X, Y, and Z axes, respectively. Torque from the engine, the weight of the battery and solar panels, and body mass all contribute to the static strain on the frame. The torque of the motor is 24.13 Nm, the battery is 29.43N, also solar panel weight 19.62N and the human's weight is 637.67N. At the center of the seat, the load was provided with a focused force of 667.08N. It is composed of human weight and battery life. The most common working torque is 24.13 N-m, as shown by the all-load ANALYSIS result. According to the total deformation, maximum stress, and factor of safety, the results are depicted in *figures 5(a) - (e)*. The maximum stress when applying torque, solar panel and sum of human and battery load is 25.05 MPa, and the smallest stress is nearly zero. The maximum deformation was 92.02 mm, and the maximum safety factor was (2.550e+008/2.505e+007) = 10.179 86 shown in *table 4*. All values were within the allowed range for a safe design.

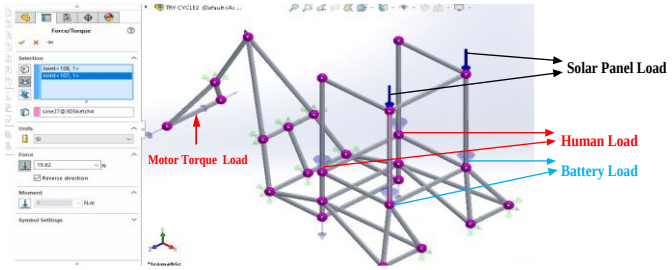

(a)

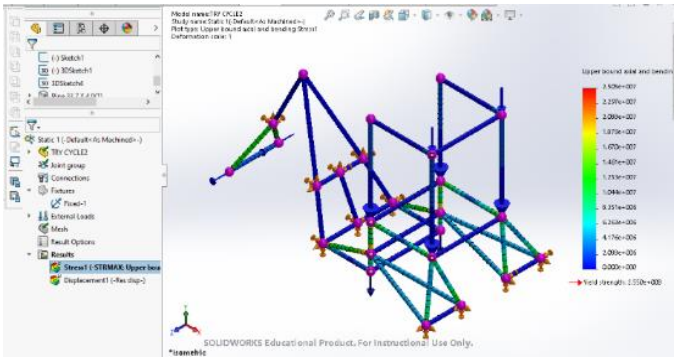

(b)

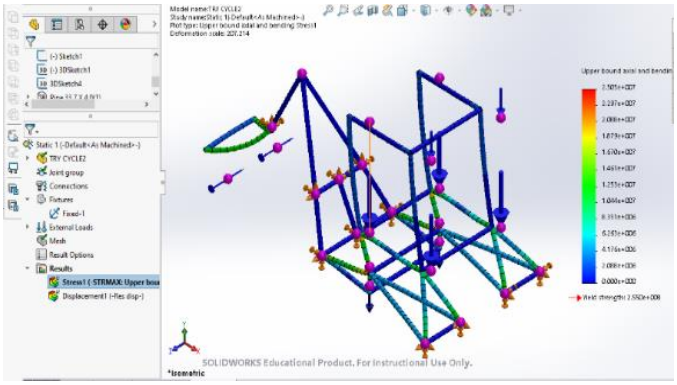

(c)

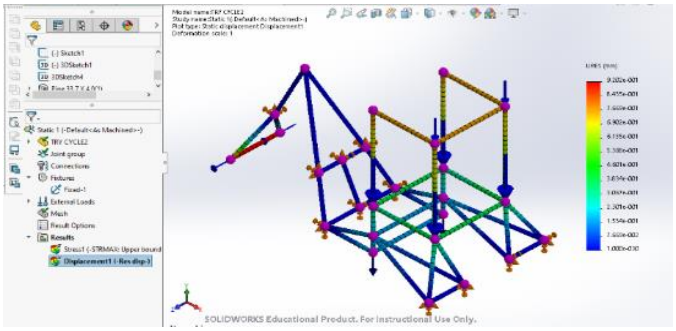

(d)

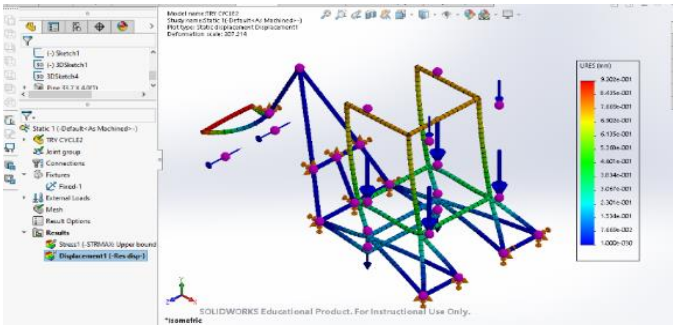

(e)

Figure 5. Sum of Solar panel, Human, battery, and Motor Torque loads (a)All load, (b) True stress (without deformation), (c) Stress with deformation (with deformation), (d) True Displacements, (e) Automatic Displacements

3.3 Comparison table of Different Loads

As listed in *table 2*, the maximum stress (MPa) is increased as the load increases and the safety factor is decreases.

Table 2. Boundary condition and Results of tricycle

Name of load	position	Direction	Maximum Stress (MPa)	Factor of safety
1. Motor Torque load	Front wheel	Positive Z- Axis	12.2	20.86
2. Sum of Human load and battery load, Motor Torque load	Sitting	Negative Y-Axis	24.48	10.41
3. Solar panel load, sum of Human load and battery load, Motor Torque load.	Top frame of sitting position	Negative Y-Axis	25.05	10.179

4. CONCLUSIONS

A solar tricycle for disabled communities was successfully constructed. The BLDC hub motor on this solar-powered tricycle provided the forward motion. The purpose of this research was to improve a conventional tricycle. Because the electric tricycle is a hybrid, it can run both electrically and pedally, providing people the same exercise as riding a tricycle. Therefore, the present disclosure offers a three-wheel hybrid electric tricycle unit that is efficient, economical, effective, and flexible for providing of an uninterruptible travelling

International Journal of Electrical and Electronics Research (IJEER)
Research Article | Volume 11, Issue 2 | Pages 465-472 | e-ISSN: 2347-470X

experience to a user by providing the capability to recharge the batteries of the locomotive itself with an automated cut-off mechanism, which would be helpful for physically challenged people. The proposed tricycle is more stable in braking turns by reducing the Centre of gravity compared to bicycle. The proposed tricycle has the movement in both directions *i.e.*, forward and reverse for disabled persons. A CAD model was created in PTC Creo 3.0, and a finite element model was generated in SolidWorks. There were two primary considerations when designing the vehicle: simplicity of design and a hybrid powertrain. Efficycle design and construction will help people to learn more environmentally friendly ways to get around.

5. ACKNOWLEDGMENTS

This manuscript research would not have been possible without the exceptional support of my supervisor, Dr. Manas Ranjan Nayak, who is a professor in the department of EE at BPUT, and my co-supervisor, Dr. B. Mangu, who is a professor in the department of EE at UCE-OU. Their enthusiasm, knowledge, and exacting attention to detail have been an inspiration and kept my work on track.

REFERENCES

[1] M. M. Abdel Wahed Ahmed and N. Abd El Monem, "Sustainable and green transportation for better quality of life case study greater Cairo–Egypt," *HBRC J.*, vol. 16, no. 1, pp. 17–37, 2020.

[2] X. Ma, I. Longley, J. Gao, and J. Salmond, "Assessing schoolchildren's exposure to air pollution during the daily commute-A systematic review," *Sci. Total Environ.*, vol. 737, p. 140389, 2020.

[3] C. D. Anderson and J. Anderson, *Electric and hybrid cars: A history*. McFarland, 2010.

[4] J. R. Babu, M. R. Nayak, and B. Mangu, "A Peer Review of Hybrid Electric Vehicle Based on Step-Up Multi-input Dc-Dc Converter and renewable energy source," in *Journal of Physics: Conference Series*, IOP Publishing, 2021, p. 012041.

[5] V. C. Shah, "Designing and investigating of electric tricycle," PhD Thesis, Kauno technologijos universitetas, 2018.

[6] K. D. Klinich, M. A. Manary, N. R. Orton, K. J. Boyle, and J. Hu, "A literature review of wheelchair transportation safety relevant to automated vehicles," *Int. J. Environ. Res. Public. Health*, vol. 19, no. 3, p. 1633, 2022.

[7] B. Stasiak-Cieślak, "Historiography of the development of the automotive industry dedicated to drivers with disabilities," *Arch. Automot. Eng. Motoryz. Vol*, vol. 98, no. 4, 2022.

[8] S. K. Pathak, P. O. Sharma, V. Goel, S. Bhattacharyya, H. Ş. Aybar, and J. P. Meyer, "A detailed review on the performance of photovoltaic/thermal system using various cooling methods," *Sustain. Energy Technol. Assess.*, vol. 51, p. 101844, 2022.

[9] S. A. Khan *et al.*, "Design of a new optimized U-shaped lightweight liquid-cooled battery thermal management system for electric vehicles: A machine learning approach," *Int. Commun. Heat Mass Transf.*, vol. 136, p. 106209, 2022.

[10] M. I. Toma, F. Gîrbacia, and C. Antonya, "A comparative evaluation of human interaction for design and assembly of 3D CAD models in desktop and immersive environments," *Int. J. Interact. Des. Manuf. IJIDeM*, vol. 6, no. 3, pp. 179–193, 2012.

[11] R. V. Petrova, *Introduction to static analysis using SolidWorks simulation*. CRC Press, 2014.

[12] S. Zetterstrom, "Electromechanical steering, suspension, drive and brake modules," in *Proceedings IEEE 56th Vehicular Technology Conference*, IEEE, 2002, pp. 1856–1863.

[13] P. Silvestri, M. Zoppi, and R. Molfino, "Dynamic investigation on a new robotized vehicle for urban freight transport," *Simul. Model. Pract. Theory*, vol. 96, p. 101938, 2019.

[14] J. Choi, K. Yi, J. Suh, and B. Ko, "Coordinated control of motor-driven power steering torque overlay and differential braking for emergency driving support," *IEEE Trans. Veh. Technol.*, vol. 63, no. 2, pp. 566–579, 2014.

[15] J. Huang *et al.*, "A hybrid electric vehicle motor cooling system—design, model, and control," *IEEE Trans. Veh. Technol.*, vol. 68, no. 5, pp. 4467–4478, 2019.

[16] G. Sevilgen, M. Kilic, H. Bayram, E. Başak, and H. Dursun, "The investigation of the innovative hybrid heat pump system designed and prototyped for heating process of electric vehicles," *Alex. Eng. J.*, vol. 68, pp. 417–435, 2023.

[17] C. L. Peterson and T. Hustrulid, "Carbon cycle for rapeseed oil biodiesel fuels," *Biomass Bioenergy*, vol. 14, no. 2, pp. 91–101, 1998.

[18] Y. Chen, Z. Wang, and Z. Zhong, "CO2 emissions, economic growth, renewable and non-renewable energy production and foreign trade in China," *Renew. Energy*, vol. 131, pp. 208–216, 2019.

[19] Aditya, Rachit Bansal, Akshit Goel, N.K. Jain and Uma Nangia (2022), Identifying and Mitigating the Barriers for Vehicle-to-Grid Adoption in India. IJEER 10(3), 447-453. DOI: 10.37391/IJEER.100307.